

## Ultrafast Population Switching of Quantum Dots in a Structured Vacuum

Xun Ma and Sajeev John

*Department of Physics, University of Toronto, 60 St. George Street, Toronto, Ontario, M5S 1A7 Canada*  
(Received 17 February 2009; revised manuscript received 29 October 2009; published 3 December 2009)

We demonstrate picosecond, high-contrast population flipping of two-level atoms interacting with femtojoule optical pulses in a 3D photonic band gap waveguide. This is the result of giant Mollow splitting caused by strong light localization and a remarkable field-dependent relaxation of the atomic Bloch vector as it evolves near an abrupt jump in the electromagnetic density of states. Unlike steady-state switching, population inversion can remain nearly complete after the pulse subsides. This may be used for multiwavelength channel, all-optical, on-chip information processing.

DOI: 10.1103/PhysRevLett.103.233601

PACS numbers: 42.50.Hz, 32.80.-t, 42.70.Qs

Photonic band gap (PBG) materials [1,2] are periodically microstructured materials that tailor the vacuum electromagnetic density of states (DOS). Reduction of DOS within the band gap facilitates light localization phenomena [3] and the inhibition of spontaneous emission [2,4]. Recent experiments with quantum dots ( $Q$  dots) [5–10] have demonstrated the strong coupling to electromagnetic fields, including vacuum Rabi splitting [5–7] and Mollow splitting [8–10] of optical transitions. In a 3D PBG material with suitable waveguide architectures, the coherent coupling of  $Q$  dots to an external field can be made several orders of magnitudes stronger [11,12]. Strong light localization in 3D PBG defects and large transition dipole moment of  $Q$  dots lead to enormous Rabi frequencies and Mollow splitting. For 3D PBG defects with mode volume much smaller than a cubic wavelength, it can be shown [13,14] that ten Terahertz (about 40 meV) of Mollow splitting are theoretically achievable, which would exceed 1% of a transition line around 1.0–1.5  $\mu\text{m}$ . This gigantic splitting may exceed the inhomogeneous linewidth of a collection of  $Q$  dots suitably embedded in a PBG structure and implies coherent dynamics on subpicosecond time scales for potential applications in ultrafast optical information processing.

In addition to enhanced coherent coupling, PBG structures can provide precipitous local DOS (LDOS) jumps that modify the strong coupling dynamics qualitatively. Resonant light-matter interaction can occur in either (A) smooth electromagnetic DOS (e.g., free space) or (B) discontinuous LDOS inside photonic crystals. The environment influences the light-matter interaction through radiative relaxation of the atomic dipole and population. According to the length of interaction time scale  $\Delta t$  (e.g., pulse duration) relative to the relaxation time scale  $1/\Gamma$ , three time regimes can be identified (Fig. 1). In (I), the coherent transient regime  $\Delta t \ll 1/\Gamma$ , transient light-matter dynamics (e.g., vacuum Rabi oscillations [15,16], adiabatic following or inversions [16–18], etc.) dominates slow dissipation. In the steady-state regime (III),  $\Delta t \gg 1/\Gamma$ , dissipation has enough time to bring the system to a steady state so that only long time behavior is important.

Resonant fluorescence is a good example [19]. In regime (II),  $\Delta t \sim 1/\Gamma$ , both the transient dynamics and the dissipation need to be taken into account. A discontinuous LDOS allows relaxation to play a much richer role during the resonant light-matter interaction. In particular, steady-state population inversion and switching of two-level systems by continuous waves (cw) has been demonstrated [12,20–23,26]. This belongs to the bottom right region in Fig. 1.

In this Letter, we identify a new strong coupling phenomena of  $Q$  dots inside a 3D PBG waveguide, which belongs to the previously unexplored  $\Delta t \sim 1/\Gamma$  region with a discontinuous LDOS. It is a remarkable high-contrast population switching mechanism based on the detailed dynamical evolution of the  $Q$  dots Bloch vector as optical pulse trains interact with the  $Q$  dots near the cutoff mode of a PBG waveguide. The LDOS divergence due to the cutoff mode band edge leads to great imbalance among the radiative decay rates of the Mollow bands induced by the driving pulse. This imbalance manifests itself as (i) an additional vacuum structure term and (ii) remarkable field-dependent spontaneous emission and dipole relaxation rates in the atomic Bloch vector equations, leading to a rapid reorientation of the Bloch vector with the driving pulse torque vector as the peak of incident pulse passes. This reorientation enables the Bloch vector to subsequently follow the trailing part of the pulse torque vector adiabatically, reaching a highly inverted state that persists long after the femtojoule, picosecond pulse subsides. This nearly full-inversion state is maintained by a

Time Regimes / DOS Profile	(I) Coherent Transient Regime ( $\Delta t \ll 1/\Gamma$ )	(II) Transient Dynamics with Decay ( $\Delta t \approx 1/\Gamma$ )	(III) Steady State Regime ( $\Delta t \gg 1/\Gamma$ )
Smooth DOS (Ordinary Vacuum)	Cavity QED; Self induced transparency; etc.	Adiabatic following/ inversion	Resonant fluorescence
Nonsmooth LDOS (Colored Vacuum)		Any new effect? Yes: Dynamic Inversion/ switching	Steady state inversion/ switching

FIG. 1. Interaction regimes for resonance quantum optics.

train of optical pulses tuned just below the atomic resonance. The inverted  $Q$  dots can be brought back to ground state using an optical pulse tuned just above the resonance. This dynamic switching mechanism is a fundamental property of the structured vacuum, unattainable in previously studied steady-state switching [12,23], and does not require chirped optical pulses as considered by others for free space adiabatic inversion [16–18].

Consider a two-level atom with transition frequency  $\omega_A$  between ground  $|1\rangle$  and excited  $|2\rangle$  states, interacting with classical laser pulse  $E(t) = \mathcal{E}(t) \cos(\omega_L t)$  with central frequency  $\omega_L$  and envelop function  $\mathcal{E}(t)$ .  $\omega_A$  is assumed to be closely above a step-shaped LDOS jump from the high LDOS region of a waveguide mode cutoff, to the low LDOS region above the cutoff edge frequency  $\omega_E$  (Fig. 2). The atom interacts with a smooth independent phonon reservoir causing dephasing. Under the rotating wave approximation [23] and in the rotation frame of  $\omega_L$ , the Hamiltonian takes the form  $H = H_S + H_R + H_{SR} + H_{\text{dephase}}$ , where  $H_S = \frac{1}{2}\hbar\Delta_{AL}\sigma_3 - \hbar\epsilon(t)(\sigma_{21} + \sigma_{12})$ ,  $H_R = \sum_{\lambda}\hbar\Delta_{\lambda}a_{\lambda}^{\dagger}a_{\lambda}$ , and  $H_{SR} = i\hbar\sum_{\lambda}g_{\lambda}(a_{\lambda}^{\dagger}\sigma_{12} - a_{\lambda}\sigma_{21})$ . Here,  $a_{\lambda}^{\dagger}$  and  $a_{\lambda}$  are the creation and annihilation operators of mode  $\lambda$  of the photonic reservoir with frequency  $\omega_{\lambda}$ . We define the bare atomic operators  $\sigma_{ij} = |i\rangle\langle j|$  ( $i, j = 1, 2$ ), population inversion  $\sigma_3 = \sigma_{22} - \sigma_{11}$ , the detunings  $\Delta_{AL} = \omega_A - \omega_L$ , and  $\Delta_{\lambda} = \omega_{\lambda} - \omega_L$ . The time-dependent Rabi frequency of the pulse is  $\epsilon(t) = d_{21}\mathcal{E}(t)/\hbar$ , assuming real dipole transition matrix element  $d_{21}$  and envelop function  $\mathcal{E}(t)$ .

The free part of the Hamiltonian  $H_S + H_R$  can be diagonalized under the time-dependent dressed state basis  $|\tilde{1}\rangle = c(t)|1\rangle + s(t)|2\rangle$  and  $|\tilde{2}\rangle = -s(t)|1\rangle + c(t)|2\rangle$ , where  $c^2(t) = \frac{1}{2}[1 + \Delta_{AL}/(2\Omega(t))]$ ,  $s^2(t) = \frac{1}{2}[1 - \Delta_{AL}/(2\Omega(t))]$  and  $\Omega(t) = \sqrt{(\Delta_{AL}/2)^2 + \epsilon(t)^2}$ . We assume the radiative decay rates for the right, left, and central Mollow sidebands are  $\gamma_{\pm}$ ,  $\gamma_0$ . In our model (see Fig. 2), the central and right Mollow bands are always in the low

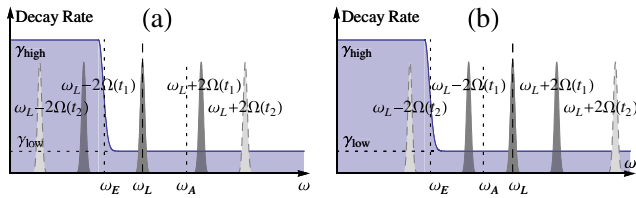


FIG. 2 (color online). Mollow bands in a step-shaped LDOS model. The central Mollow band at  $\omega_L$  has a fixed decay rate  $\gamma_0 = \gamma_{\text{low}}$ . The time-dependent right Mollow side band at  $\omega_L + 2\Omega(t)$  is shown at time  $t_1$  when  $\epsilon(t_1)$  is small (dark shaded peak) and  $t_2$  when  $\epsilon(t_2)$  is big (light shaded peak), with fixed decay rate  $\gamma_+ = \gamma_{\text{low}}$ . For the left Mollow side band  $\omega_L - 2\Omega(t)$ : (a)  $\Delta_{AL} > 0$  and  $|\Delta_{AL}| > \Delta_{LE}$ . The left side band always resides in high LDOS region with  $\gamma_- = \gamma_{\text{high}}$ . (b)  $\Delta_{AL} < 0$  and with  $|\Delta_{AL}| < \Delta_{LE}$ . The left side band moves from low LDOS region with  $\gamma_- = \gamma_{\text{low}}$  at  $t_1$  (dark shaded peak), to high LDOS region with  $\gamma_- = \gamma_{\text{high}}$  at  $t_2$  (light shaded peak).

LDOS region with a decay rate  $\gamma_{\text{low}}$ , meaning  $\gamma_0 = \gamma_+ \equiv \gamma_{\text{low}}$ . The left Mollow side band, however, can be in either the low LDOS region or the high LDOS region with a decay rate  $\gamma_{\text{high}}$ , depending on the relative size of the Mollow splitting  $2\Omega(t)$  and the detuning  $\Delta_{LE} = \omega_L - \omega_E$ . For the two situations considered, Fig. 2(a) corresponds to  $\Delta_{AL} > \Delta_{LE} > 0$  so that  $2\Omega(t) \geq \Delta_{AL} > \Delta_{LE}$  and the left Mollow side band experiences a constant decay rate  $\gamma_- = \gamma_{\text{high}}$ . Figure 2(b) corresponds to  $\Delta_{AL} < 0$  and  $|\Delta_{AL}| < \Delta_{LE}$  so that as  $\epsilon(t)$  changes, the left Mollow side band can move between the low LDOS region with  $\gamma_- = \gamma_{\text{low}}$  and the high LDOS region with  $\gamma_- = \gamma_{\text{high}}$ .

In the Born-Markov approximation [21], the radiative part of the master equation can be derived in the interaction picture and the dressed state basis [14,23]. We now consider the complete master equation for the atomic density matrix, including a phonon dephasing rate  $\gamma_p$ , in the Schrödinger picture and bare atomic basis. Defining  $\sigma_1 = \sigma_{12} + \sigma_{21}$  for the in-phase part and  $\sigma_2 = i(\sigma_{12} - \sigma_{21})$  for the in-quadrature part of the atomic dipole moment, we obtain the Bloch equation associated with the full non-secular master equation [13,14]:

$$\dot{\rho} = \mathbf{\Omega} \times \rho - \mathbf{\Gamma}_\rho + \mathbf{C}. \quad (1)$$

Here, the Bloch vector  $\rho \equiv (\langle\sigma_1\rangle, \langle\sigma_2\rangle, \langle\sigma_3\rangle) \equiv (u, v, w)$  describes a “mixed” state and is free to evolve anywhere inside the unit sphere  $u^2 + v^2 + w^2 \leq 1$ . The angular brackets denote a trace of the atomic operators with respect to the time-dependent atomic density operator. The coherent driving of  $\rho$  by the incident pulse is described by the torque vector  $\mathbf{\Omega} \equiv (\Omega_u, \Omega_v, \Omega_w) \equiv (-2\epsilon, 0, \Delta_{AL})$ . The influence of the vacuum LDOS discontinuity appears partly in the form of the decay term  $\mathbf{\Gamma}_\rho \equiv (u/T_u, v/T_v, w/T_w)$ . The decay rates  $1/T_{u,v} \equiv \frac{c^2(1+s^2)\gamma_+ + s^4\gamma_- + 4\gamma_p}{2} \mp \frac{c^2s^2(\gamma_+ - \gamma_-)}{2}$  and  $1/T_w \equiv c^2(1 + s^2)\gamma_+ + s^4\gamma_-$  are field- and correspondingly time-dependent in sharp contrast to the constant decay rates in ordinary vacuum. Yet the most striking influence from the electromagnetic vacuum structure is on the driving vector  $\mathbf{C} \equiv (V, 0, -1/T_w + Vu)$ . Because of the imbalance between the Mollow band decay rates, the shifted detailed balance among the dressed levels creates a “dragging” on the Bloch vector towards the  $u < 0$  and  $w > 0$  direction described by the unique “vacuum structure term”  $V \equiv (\gamma_+ - \gamma_-)cs^3$  not observable in ordinary vacuum.

The Bloch vector dynamics described by Eq. (1) is dramatically different from that in ordinary vacuum. In particular, if  $\epsilon(t) = \epsilon_0$  is a constant (cw laser), then by setting  $\dot{\rho} = 0$ , we can obtain the steady-state solution  $(u_{\text{ss}}, v_{\text{ss}}, w_{\text{ss}})$  of Eq. (1) [13,14]. If we assume  $\Delta_{AL} > \Delta_{LE} > 0$  [Fig. 2(a)], so that  $\gamma_- \equiv \gamma_{\text{high}}$  and  $\gamma_+ \equiv \gamma_{\text{low}}$ , then  $(u_{\text{ss}}, v_{\text{ss}}, w_{\text{ss}})$  shows switching and weak inversion of the population  $w_{\text{ss}}$  [13,14] at threshold Rabi frequencies  $\epsilon_{\text{thr}}$  that are proportional to  $\Delta_{AL}$  and vary for different decay rates  $\gamma_-/\gamma_+$  and dephasing rates  $\gamma_p$ .

For a pulsed driving beam,  $(u_{ss}, v_{ss}, w_{ss})$  can be interpreted as the instantaneous steady state  $\rho_{ss}^{inst}(\epsilon(t'))$  at time  $t'$  by setting  $\epsilon_0 = \epsilon(t')$ . As  $\epsilon(t')$  changes over time,  $\rho_{ss}^{inst}(\epsilon(t'))$  changes accordingly. The true Bloch vector  $\rho(t')$  has a tendency to decay towards  $\rho_{ss}^{inst}(\epsilon(t'))$  at every moment  $t'$ . However, the evolution path of  $\rho$  can be very different from that of  $\rho_{ss}^{inst}$ , since the transient decay of  $\rho$  may not be fast enough to allow  $\rho$  to catch up the movement of  $\rho_{ss}^{inst}$ . We now show that for suitable pulses, the relaxation rate [roughly characterized as  $|\Gamma| = |(1/T_u, 1/T_v, 1/T_w)|$ ] of  $\rho$  toward  $\rho_{ss}^{inst}$  is fast enough at the pulse peak to let  $\rho$  catch up  $\rho_{ss}^{inst}$ . Then, the weak inversion property of  $\rho_{ss}^{inst}$  at this catch up point leads to a dramatic rotation of the Bloch vector from nearly antiparallel to nearly parallel to  $\Omega$ . The subsequent adiabatic following of the torque vector by the Bloch vector as the pulse amplitude subsides leads to the evolution of the Bloch vector from the weakly inverted state  $\rho_{ss}^{inst}$  to a nearly completely inverted state. In the absence of vacuum structure,  $\rho$  remains roughly antiparallel to  $\Omega$  and simply returns to the ground state as the pulse subsides.

Consider a pulse with  $\Delta_{AL} > 0$  and Gaussian profile  $\epsilon(t) = \epsilon_p \exp[-(\frac{t-t_p}{\tau})^2]$ . The relaxation rate  $|\Gamma|$  [Fig. 3(b)] increases with  $\epsilon$ , while the  $\rho_{ss}^{inst}$  speed  $|d\rho_{ss}^{inst}/dt| = |d\rho_{ss}^{inst}/d\epsilon \cdot d\epsilon/dt|$  decreases significantly below  $|\Gamma|$  for  $\epsilon > \epsilon_{thr}$ . If the pulse is strong enough so that its peak Rabi frequency  $\epsilon_p \gg \epsilon_{thr}$ , then the relaxation of  $\rho$  to  $\rho_{ss}^{inst}$  is very fast compared to the motion of  $\rho_{ss}^{inst}$  near the pulse peak at time  $t_p$ , over a time  $\tau_{qs}$  called the steady-state

attraction interval. If  $\tau_{qs}$  is longer than the average lifetime  $1/|\bar{\Gamma}|$  during  $\tau_{qs}$ , then  $\rho$  has enough time to align with  $\rho_{ss}^{inst}$  during  $\tau_{qs}$ , provided that

$$|d\rho_{ss}^{inst}(t)/dt| \ll |\Gamma| \quad \text{for } \tau_{qs} \gg 1/|\bar{\Gamma}|. \quad (2)$$

Figure 3(a) shows the 3D evolution path of  $\rho$  (solid curve) and  $\rho_{ss}^{inst}$  (dotted curve). Since the pulse satisfies the steady-state attraction condition Eq. (2),  $\rho(t_1)$  is able to catch up  $\rho_{ss}^{inst}(t_1)$  through field-enhanced decay. During this catch up process, the Bloch vector flips from antiparallel to parallel alignment with the torque vector  $\Omega$  (see [13,14] for detail). If the incident optical pulse further satisfies the adiabatic condition  $d\epsilon(t)/dt \ll |\Omega| \cdot |\Delta_{AL}|$ , then from  $t_1$  to  $t_3$ ,  $\rho$  will adiabatically follow the movement of the torque vector from  $\Omega(t_1)$  to  $\Omega(t_3)$ . Since  $\Omega$  points in the  $w > 0$  direction,  $\rho$  can reach a highly inverted state  $\rho(t_3)$ . During this adiabatic following step, the evolution of  $\rho(t)$  deviates again from that of  $\rho_{ss}^{inst}(t)$  because the inequality  $|d\rho_{ss}^{inst}/dt| \ll |\Gamma|$  is violated as the pulse subsides due to the declining field-dependent relaxation rate. This slow relaxation prevents the Bloch vector from decaying back to the ground state like  $\rho_{ss}^{inst}$ . As the relaxation rate changes with field strength, the interacting light-matter system essentially alternates between steady-state time regime (III) and adiabatic following dynamics in coherent transient regime (I) (Fig. 1). For small phonon dephasing  $\gamma_p \ll \gamma_-$  and  $\gamma_+ \ll \gamma_-$ , the atom achieves nearly complete inversion  $w_{max} \approx 1$ .  $w_{max}$  decreases as  $\gamma_p$  increases. Importantly, the initial condition of the Bloch vector  $\rho(t_0)$  has relatively small influence on the highly inverted state achieved. During the steady-state attraction process, most information about the initial Bloch vector is erased. Our dynamic inversion is a structured vacuum variant of the adiabatic inversion in ordinary vacuum, without any effective chirping in  $\Delta_{AL}$  during the pulse [16–18].

Figure 3(c) depicts switching down of an inverted atom back to the ground state using an oppositely detuned ( $\Delta_{AL} < 0$ ) optical pulse [Fig. 2(b)]. Since the steady-state solution  $\rho_{ss}^{inst}$  presents no inversion for  $\Delta_{AL} < 0$ ,  $\rho(t)$  is attracted to  $\rho_{ss}^{inst}(t_1)$  below the  $u-v$  plane. After parallel alignment with  $\Omega(t_1)$ ,  $\rho(t)$  adiabatically follows  $\Omega(t)$  in the  $w < 0$  direction to the ground state  $\rho(t_3)$ . Here, the sudden change of  $\gamma_-$  between  $\gamma_{low}$  and  $\gamma_{high}$  near the LDOS jump [see Fig. 2(b)] leads to some artificial kinks in the overall Bloch vector trajectory [Fig. 3(c)].

Based on the unusual strong coupling dynamics described above, we now illustrate a multichannel switching device, whose gate and holding fields consist of a train of picosecond control pulses in a given wavelength channel 1 ( $L_1$ ) that maintain population inversion of an inhomogeneously broadened collection of independent  $Q$  dots. This can be used to amplify signal pulses in various other wavelength channels until a control pulse in wavelength channel 2 ( $L_2$ ) arrives to deexcite the  $Q$  dots. The inset of Fig. 4 depicts the spectral configuration of the device. The two-level atoms have a Gaussian distribution (black peak)

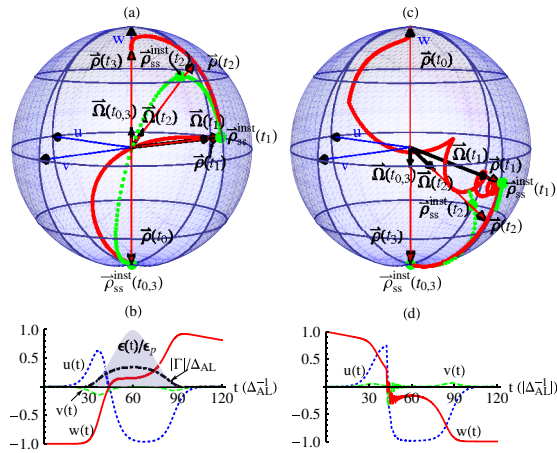


FIG. 3 (color online). Dynamical population inversion when  $\Delta_{AL} > 0$  (a), (b) and deexcitation when  $\Delta_{AL} < 0$  (c), (d) of a two-level atom.  $\gamma_- = 1.25\Delta_{AL}$ ,  $\gamma_-/\gamma_+ = 500$ ,  $\gamma_p = 0$ ,  $\Delta_{LE} = 0.5\Delta_{AL}$ ,  $\epsilon_p = 3\Delta_{AL} \ll \epsilon_{thr}$ ,  $t_1 = 65\Delta_{AL}^{-1}$ ,  $t_2 = 85\Delta_{AL}^{-1}$ ,  $t_3 = 120\Delta_{AL}^{-1}$ ,  $\tau = 30\Delta_{AL}^{-1}$ . (a), (c) Three-dimensional evolution path of the Bloch vector  $\rho(t)$  [(red) solid curve]. The thin (red) vectors are Bloch vectors at  $t_{0,1,2,3}$ , while the thick vectors are the corresponding torque vectors. The big (green) dots are the instantaneous steady states at  $t_{0,1,2,3}$ , while the dotted (green) curve shows the evolution path of the instantaneous steady states  $\rho_{ss}^{inst}(t)$ ; (b), (d) Two-dimensional plot of  $u(t)$ ,  $v(t)$ ,  $w(t)$ , scaled pulse profile  $\epsilon(t)/\epsilon_p$ , and relaxation rate  $|\Gamma|/\Delta_{AL}$ .

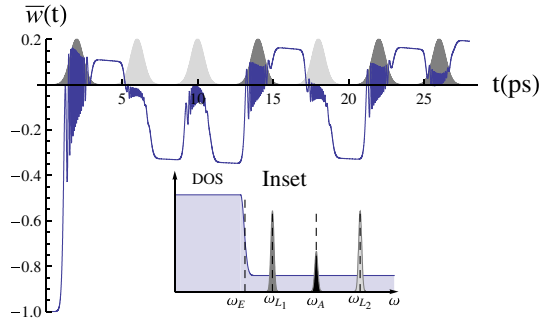


FIG. 4 (color online). Optical pulse train controlled average population  $\bar{w}(t)$  (solid curve) of inhomogeneously broadened atomic distribution with phonon dephasing, and the scaled temporal profiles of the pulses in channel 1 (dark shading) and channel 2 (light shading). All pulses have a FWHM of  $\tau = 1$  ps and peak Rabi frequency  $\epsilon_p = 42$  THz. The switching contrast of  $\bar{w}$  is about 0.5; *Inset*: Schematic spectral model of the switching device.  $\Delta_{L_1 E} = 5$  THz,  $\Delta_{AL_1} = 8$  THz,  $\Delta_{AL_2} = -8$  THz, and inhomogeneous width  $\Delta\omega_A/\omega_A \approx 1\%$ . The decay rates are  $\gamma_{\text{high}} = 2.5$  THz ( $\gamma_{\text{high}}^{-1} = 0.4$  ps),  $\gamma_{\text{low}} = 0.005$  THz, and  $\gamma_p = 0.5$  THz.

with average transition frequency  $\bar{\omega}_A$  and FWHM  $\Delta\omega_A = 12$  THz ( $\Delta\omega_A/\omega_A \approx 0.6\%$  for current GaAs based  $Q$  dots with  $\lambda \sim 1 \mu\text{m}$ , but can easily reach 1% for  $Q$  dots with longer transitions wavelength). Channel 1 (dark peak) has central frequency  $\omega_{L_1}$  with  $\Delta_{AL_1} = \bar{\omega}_A - \omega_{L_1} = 8$  THz, while channel 2 (light peak) has central frequency  $\omega_{L_2}$  with  $\Delta_{AL_2} = -8$  THz. We consider device operation with a phonon dephasing rate  $\gamma_p = 0.5$  THz. As shown in Fig. 4, a train of Gaussian pulses in channel 1 with FWHM 1 ps (dark peaks) causes Mollow splitting of the atoms, keeping the left Mollow side bands in the high LDOS region [Fig. 2(a)] with average population inversion  $\bar{w} > 0$ . A pulse in channel 2 (light peaks) moves the left Mollow side bands in and out of the high LDOS region [Fig. 2(b)], thereby switching the atoms to an uninverted state with  $\bar{w} < 0$ . A stable population switching contrast as high as 0.5 is achieved.

After the passage of a control pulse in Channel 1,  $\bar{w}$  stays inverted with slow decay rate  $\gamma_{\text{low}}$ . If a subsequent weak signal pulse (with area  $\pi$ ) in a third resonant channel (centered at  $\bar{\omega}_A$ ) passes through this amplifying medium, pulse transmission and reshaping is equivalent to that of an amplifying medium in ordinary vacuum [16,24] (provided the signal pulse is not so strong as to push the Mollow sidebands back into the high LDOS region). With an additional broadband linear loss, signal pulses will be amplified into stable  $\pi$  pulse solitons and traverse the device without attenuation. On the other hand, a control pulse in channel 2 leaves  $\bar{w}$  uninverted. A subsequent signal  $\pi$  pulse is then completely absorbed according to McCall-Hahn area theorem [16,25]. Effectively, we can control light with light.

For a typical quantum dot dipole moment around  $10^{-28}$  C m,  $\epsilon_p = 42$  THz corresponds to a peak field strength on the order of  $10^5$  V/cm. However, this strong

field persists only on subpicosecond time scales, and the non-Markovian effects not completely captured in our model are expected to considerably lower the required field strength [22]. The pulse energy per switching operation is on the order of femtojoules, with submilliWatt average operating power [14].

In summary, we have identified vacuum structure terms in the optical Bloch vector equation for a coherently driven quantum dot in a PBG material. These new terms enable unprecedented control over quantum dot nonlinear dynamics and allow the optical Bloch vector to explore the full upper half of the Bloch sphere. The 3D PBG waveguide facilitates strong light localization, resulting in enormous Mollow splittings exceeding the inhomogeneous line width at modest power levels. This offers a foundation for an on-chip multichannel all-optical transistor. Unlike electronic binary logic and quantum probabilistic multivalued logic, our optical system offers the possibility of picosecond deterministic multivalued logic.

This work was supported in part by the Natural Sciences and Engineering Research Council of Canada.

- [1] S. John, Phys. Rev. Lett. **58**, 2486 (1987).
- [2] E. Yablonovitch, Phys. Rev. Lett. **58**, 2059 (1987).
- [3] S. John, Phys. Rev. Lett. **53**, 2169 (1984).
- [4] S. John and J. Wang, Phys. Rev. Lett. **64**, 2418 (1990).
- [5] T. Yoshie and A. Scherer *et al.*, Nature (London) **432**, 200 (2004).
- [6] J. P. Reithmaier and G. Sek *et al.*, Nature (London) **432**, 197 (2004).
- [7] E. Peter *et al.*, Phys. Rev. Lett. **95**, 067401 (2005).
- [8] Xiaodong Xu and Bo Sun *et al.*, Science **317**, 929 (2007).
- [9] A. N. Vamivakas and Y. Zhao *et al.*, Nature Phys. **5**, 198 (2009).
- [10] E. B. Flagg and A. Muller *et al.*, Nature Phys. **5**, 203 (2009).
- [11] R. Wang and S. John, Phys. Rev. A **70**, 043805 (2004).
- [12] D. Vujic and S. John, Phys. Rev. A **76**, 063814 (2007).
- [13] See EPAPS Document No. E-PRLTAO-103-040950 for the derivation and steady-state solution of the Bloch equation and discussion of the Mollow splitting size. For more information on EPAPS, see <http://www.aip.org/pubservs/epaps.html>.
- [14] X. Ma and S. John, Phys. Rev. A (to be published).
- [15] I. I. Rabi, Phys. Rev. **51**, 652 (1937).
- [16] L. Allen and J. H. Eberly, *Optical Resonance and Two level Atoms* (John Wiley & Sons, Inc., New York, 1975).
- [17] E. B. Treacy, Phys. Lett. A **27**, 421 (1968).
- [18] M. M. T. Loy, Phys. Rev. Lett. **32**, 814 (1974).
- [19] B. R. Mollow, Phys. Rev. **188**, 1969 (1969).
- [20] S. John and M. Florescu, J. Opt. A **3**, S103 (2001).
- [21] S. John and T. Quang, Phys. Rev. Lett. **78**, 1888 (1997).
- [22] M. Florescu and S. John, Phys. Rev. A **64**, 033801 (2001).
- [23] M. Florescu and S. John, Phys. Rev. A **69**, 053810 (2004).
- [24] V. S. Letokhov, Sov. Phys. JETP **29**, 221 (1969).
- [25] S. L. McCall and E. L. Hahn, Phys. Rev. Lett. **18**, 908 (1967).
- [26] T. W. Mossberg and M. Lewenstein, J. Opt. Soc. Am. B **10**, 340 (1993).